Radiobiologic Optimization of Combination Radiopharmaceutical Therapy Applied to Myeloablative Treatment of Non-Hodgkin Lymphoma

Robert F. Hobbs, Richard L. Wahl, Eric C. Frey, Yvette Kasamon, Hong Song, Peng Huang, Richard J. Jones, and George Sgouros

Johns Hopkins University, Baltimore Maryland

Combination treatment is a hallmark of cancer therapy. Although the rationale for combination radiopharmaceutical therapy was described in the mid-1990s, such treatment strategies have only been implemented clinically recently and without a rigorous methodology for treatment optimization. Radiobiologic and quantitative imaging-based dosimetry tools are now available that enable rational implementation of combined targeted radiopharmaceutical therapy. Optimal implementation should simultaneously account for radiobiologic normal-organ tolerance while optimizing the ratio of 2 different radiopharmaceuticals required to maximize tumor control. We have developed such a methodology and applied it to hypothetical myeloablative treatment of non-Hodgkin lymphoma (NHL) patients using ^{131}I-tositumomab and ^{90}Y-ibritumomab tiuxetan. **Methods:** The range of potential administered activities (AAs) is limited by the normal-organ maximum-tolerated biologic effective doses (MTBEDs) arising from the combined radiopharmaceuticals. Dose-limiting normal organs are expected to be the lungs for ^{131}I-tositumomab and the liver for ^{90}Y-ibritumomab tiuxetan in myeloablative NHL treatment regimens. By plotting the limiting normal-organ constraints as a function of the AAs and calculating tumor biologic effective dose (BED) along the normal-organ MTBED limits, we obtained the optimal combination of activities. The model was tested using previously acquired patient normal-organ and tumor kinetic data and MTBED values taken from the literature. **Results:** The average AA value based solely on normal-organ constraints was 19.0 ± 8.2 GBq (range, 3.9–36.9 GBq) for ^{131}I-tositumomab and 2.77 ± 1.64 GBq (range, 0.42–7.54 GBq) for ^{90}Y-ibritumomab tiuxetan. Tumor BED optimization results were calculated and plotted as a function of AA for 5 different cases, established using patient normal-organ kinetics for the 2 radiopharmaceuticals. Results included AA ranges that would deliver 95% of the maximum tumor BED, allowing for informed inclusion of clinical considerations, such as a maximum-allowable ^{131}I administration. **Conclusion:** A rational approach for combination radiopharmaceutical treatment has been developed within the framework of a proven 3-dimensional (3D) personalized dosimetry software, 3D-RD, and applied to the myeloablative treatment of NHL. We anticipate that combined radioisotope therapy will ultimately supplant single radioisotope therapy, much as combination chemotherapy has substantially replaced single-agent chemotherapy.

Received Nov. 30, 2012; revision accepted Apr. 8, 2013.

For correspondence or reprints contact: Robert F. Hobbs, Department of Radiology, Johns Hopkins University, School of Medicine, CRB II 4M.60, 1550 Orleans St., Baltimore MD 21231.

E-mail: rhobbs3@jhmi.edu

Published online Aug. 5, 2013.

Key Words: radiopharmaceutical therapy; dosimetry; treatment planning; BED; lymphoma

J Nucl Med 2013; 54:1535–1542
DOI: 10.2967/jnumed.112.117952

Combination chemotherapy is the mainstay of lymphoma treatment. In contrast, despite more than 25 years of clinical study and several theoretic studies (*1–3*), radiopharmaceutical therapies have only recently been combined in a clinical trial (*4–8*)—principally because of the technical difficulties and concerns over toxicity (*9*)—and such treatment strategies have only been implemented clinically recently and without a rigorous methodology for treatment optimization.

Anti-CD20–targeted monoclonal antibodies, both unlabeled and radiolabeled, are active agents in the treatment of B-cell lymphomas (*10*). The unlabeled monoclonal antibody rituximab mediates its therapeutic effects through several mechanisms including antibody-dependent cellular cytotoxicity, complement-fixation, and the direct induction of apoptosis (*11*). The addition of radioactivity to the anti-CD20 antibody has been shown to increase response rates and therapeutic efficacy over the unlabeled antibody alone in several trials (*12*). The 2 Food and Drug Administration–approved radioimmunotherapies for lymphoma, ^{131}I-tositumomab plus unlabeled tositumomab (Bexxar therapeutic regimen; GlaxoSmithKline) and rituximab plus ^{90}Y-ibritumomab tiuxetan (Zevalin; Spectrum Pharmaceuticals), are effective therapies for follicular lymphomas; however, their administered radioactivity doses, and quite likely their efficacy, are limited by hematopoietic toxicity.

High-dose single-agent radioimmunotherapy with ^{131}I-tositumomab with autologous stem cell support was introduced by Press et al. more than 2 decades ago (*13*): they were able to achieve high response rates and manageable nonhematopoietic toxicity. More recently, ^{90}Y-ibrutumomab tiuxetan has also been used in clinical trials in conjunction with blood or marrow transplantation without excess toxicity (*14*). Individualized patient dosimetry to determine the administered activity (AA) required to deliver tolerable normal-organ absorbed doses was essential to the safe conduct of these trials (*15*).

The combination of ^{131}I-tositumomab and ^{90}Y-ibritumomab tiuxetan in a myeloablative regime has the potential to substantially increase efficacy for the following 2 reasons: the combination may target a wider range of tumor diameters, given the different mean path lengths of β-particles for the respective isotopes

(~1 mm with ^{131}I, ~3–5 mm with ^{90}Y) (*2*); and the radiopharmaceuticals have orthogonal toxicity (predominantly lungs and kidneys from ^{131}I-tositumomab and liver from ^{90}Y-ibritumomab tiuxetan) (*16,17*), which may permit a greater total absorbed dose to the targets (tumors). However, there are several limitations in the currently available combination models, which the methodology presented here seeks to address. First, the current combination methodologies are based on criteria that limit the maximum-tolerated absorbed dose (MTD) for the organs at risk (*9*). However, it has been shown that the relevant dosimetric quantity related to toxicity in normal organs (*18*) is the biologic effective dose (BED). Therefore, a model based on maximum-tolerated BED (MTBED) constraints would be preferable. This approach is especially important for therapies combining 2 radionuclides because the dose rates are different. Second, the endpoint of the proposed model (i.e., the quantity that is maximized) is the tumor BED or, for a patient with multiple tumors (which is often the case for this disease), the equivalent uniform biologic effective dose (EUBED), which has also shown promise as a relevant quantity for tumor response. Finally, the present methodology has been developed in the context of a personalized 3-dimensional (3D) dosimetry package, 3D-RD, with the objective and the proven ability to be implemented clinically in real time (*19*).

MATERIALS AND METHODS

Overview

The method presented here optimizes the administration of ^{131}I-tositumomab and ^{90}Y-ibritumomab tiuxetan for treatment of lymphoma at myeloablative doses. It may be generalized to any combination of therapeutics whose toxicities are orthogonal. It is dosimetrically driven and, more specifically, founded on radiobiologic modeling and the linear-quadratic formalism. The methodologic steps are as follows. First, establish the equations for limiting toxicities based on limiting normal-organ BED; this is an extension of previous work (*9*) using absorbed dose and treatment to both MTDs. Next, instead of focusing solely on toxicity, seek to optimize response by maximizing the tumor BED while respecting the established normal-organ constraints. Finally, extend the optimization to multiple tumors by calculating the disease EUBED.

Normal-Organ Absorbed Dose Constraints

Mathematic modeling for the constraints imposed by normal-organ toxicity for combined radioimmunotherapy has been previously developed (*9*) in the context of nonmyeloablative neuroendocrine tumor therapy. For NHL, the typical constraints for myeloablative ^{131}I-tositumomab, or Bexxar (*B*) and ^{90}Y-ibritumomab tiuxetan, or Zevalin (*Z*) are the lungs (*lu*) and liver (*li*), respectively, with kidneys (*ki*) as a possible concern for Bexxar. A system of 2 equations and 2 unknowns can be set up and solved for the amount of injected activities of ^{131}I-tositumomab, A_B, and ^{90}Y-ibritumomab tiuxetan, A_Z, using this formalism and given the MTD constraint values and the dose per unit of AA of agent A ($A = Z$ or B), $d_{A,O}$, to the dose limiting organ O ($O = lu$ or li):

$$\begin{cases} MTD_{lu} = A_Z d_{Z,lu} + A_B d_{B,lu} \\ MTD_{li} = A_Z d_{Z,li} + A_B d_{B,li} \end{cases}. \qquad \text{Eq. 1}$$

Although the equations in Equation 1 allow for any mathematic solution, additional physical constraints are imposed, namely, the AAs must be positive and the total absorbed dose to kidneys must not exceed the threshold for renal toxicity. Strictly speaking, both equations should be written as inequalities. However, it is clear that from an optimization standpoint, the limiting values are the ones of interest. Because the MTD and d values are positive, it is not possible for both A_Z and A_B to be negative solutions to Equation 1; an optimal solution will exist if both activities are positive. An example of this formalism is illustrated graphically in Figure 1A using d values taken from previously published patient data for ^{131}I-tositumomab (*20*) and ^{90}Y-ibritumomab tiuxetan (*21*), as are all the examples in this manuscript. An MTD value of 27 Gy was chosen for both the liver and the lungs (*19*).

BED Constraints

The BED (*22*) relates absorbed dose and absorbed dose rate to the biologic effect it would have if the total absorbed dose were delivered at an infinitesimally low dose rate. As validation of its biologic importance, the BED has been shown to be predictive of toxicity thresholds in normal organs (*18*). Consequently, a model that incorporates

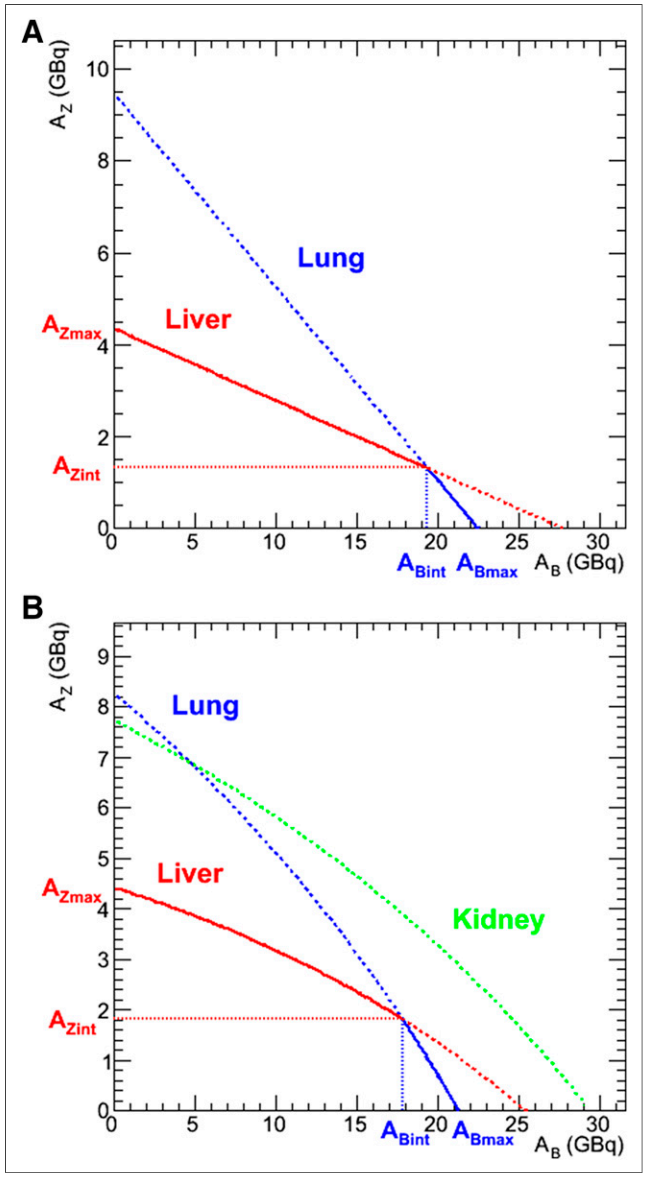

FIGURE 1. Optimization based on normal-organ MTD (A; Eq. 1) and MTBED (B; Eqs. 6 or 8) constraints in A_B vs. A_Z plots. Blue line shows lung, red line shows liver, and green line shows kidney constraints. Lines are solid when they represent the activity-limiting constraint; dotted line constraints are automatically satisfied by solid line criteria.

radiobiology and more specifically the BED into its constraints is more likely to be successful in limiting toxicity. The formula for the BED is:

$$BED = D\left(1 + \frac{G(\infty)}{\alpha/\beta} \times D\right), \quad \text{Eq. 2}$$

where α and β are the organ-specific radiobiologic parameters from the linear quadratic model of cell survival (*23*), D is the absorbed dose, and $G(\infty)$ is the Lea–Catcheside G-factor:

$$G(\infty) = \frac{2}{D^2} \times \int_0^\infty \dot{D}(t)dt \int_0^t \dot{D}(w) \times e^{-\mu(t-w)}dw. \quad \text{Eq. 3}$$

Here μ is the DNA repair constant, assuming exponential repair, and t and w are integration variables. For a simple exponential fit of the dose rate, $\dot{D}$, as a function of time

$$\dot{D}(t) = \dot{D}_0 e^{-\lambda t}, \quad \text{Eq. 4}$$

which is typical for normal-organ kinetics for both ^{131}I-tositumomab and ^{90}Y-ibritumomab tiuxetan individually, the G-factor reduces to:

$$\frac{\lambda}{\lambda + \mu}, \quad \text{Eq. 5}$$

where λ is the exponential dose rate decay rate from Equation 4. The normal-organ MTBED values constrain the 2 AAs, A_Z and A_B, according to the following formulae:

$$MTBED_i = \left(A_Z d_{Z,i} + A_B d_{B,i}\right)\left(1 + G(\infty)_i \times \frac{A_Z d_{Z,i} + A_B d_{B,i}}{\alpha_i/\beta_i}\right), \quad \text{Eq. 6}$$

where the index i can stand for any dose-limiting organ, and the $d_{A,i}$ values still represent the absorbed dose per unit activity for Bexxar ($A = B$) or Zevalin ($A = Z$) for the respective organ i. The dose rate is now a sum of the 2 (B and Z) exponential dose rate functions and no longer a simple exponential. The G-factor thus becomes:

$$G(\infty)_i = \frac{1}{\left(A_Z d_{Z,i} + A_B d_{B,i}\right)^2}\left(\frac{A_Z^2 d_{Z,i}^2 \lambda_{Z,i}}{\lambda_{Z,i} + \mu_i} + \frac{A_B^2 d_{B,i}^2 \lambda_{B,i}}{\lambda_{B,i} + \mu_i}\right). \quad \text{Eq. 7}$$

The values used for the α/β and μ parameters are given in Table 1 and are taken from the literature.

Equation 6 is quadratic in A_Z (and A_B). By solving for A_Z and plotting as a function of A_B (or vice versa), we obtained a graphical representation of Equation 6; these are shown in Figure 1B using the same measured patient parameters as for Figure 1A but with MTBED constraints of 30 Gy for the lungs and 35 Gy for the liver. We have included the kidneys as a possible limiting organ although in this illustrative example the kidney constraints will always be met if the lung and liver constraints are met. The equations derived from Equation 6 that are graphed in Figure 1B are:

$$A_Z = \frac{(\lambda_{Z,i} + \mu_i)\alpha_i/\beta_i}{2\lambda_{Z,i} d_{Z,i}^2}\left(-d_{Z,i} + \sqrt{d_{Z,i}^2 - 4\frac{\lambda_{Z,i} d_{Z,i}^2}{(\lambda_{Z,i} + \mu_i)\alpha_i/\beta_i}\left(A_B d_{B,i} + \frac{\lambda_{B,i} A_B^2 d_{B,i}^2}{(\lambda_{B,i} + \mu_i)\alpha_i/\beta_i} - MTBED_i\right)}\right), \quad \text{Eq. 8}$$

where the index i can stand for any dose-limiting organ (lungs, liver, and kidneys in Fig. 1B).

The limiting constraints are shown in solid color in Figure 1: any combination of A_B and A_Z whose corresponding point on the graph is located within the bounds of the 2 axes and the solid colored lines will deliver a dose (or BED) less than or equal to the MTD (or MTBED) to both organs. Concretely, in the case where a combination of 2 BED-based constraints (lungs and liver, as illustrated in Fig. 1B) are used, the intersection of the 2 curves (A_{Bint}, A_{Zint}) may be found by setting Equation 8 for liver (*li*) equal to Equation 8 for lungs (*lu*), solving for A_B and then substituting this value of A_B into the version of Equation 8 for either organ to find A_Z. These activity values (A_{Bint}, A_{Zint}) from the intersection point will deliver the MTBED to both organs, lungs and liver. In theory, an algebraic formulation of A_{Bint} (and A_{Zint}) may be derived; however, the formula is a fourth-order polynomial and it is much simpler to arrive at the solution numerically.

The intersection values for A_B and A_Z maximize the BED to the constraining organs, but it does not necessarily follow that those are the desired or optimal activities to administer, because normal organs are not the target of the radiopharmaceutical therapy. Ultimately, a dosimetric quantity that translates the effect of the AAs on the target, that is, the tumors, is the quantity that should be maximized. Intuitively, the intersection point represents a probable good first-order estimate of this optimization point. However, for a more rigorous optimization, the target quantity to be maximized needs to be determined and then calculated and plotted as a function of A_B and A_Z taken along the solid path plotted in Figure 1B. The application of this concept is demonstrated using the tumor BED and the disease EUBED for multiple tumors.

Tumor BED Optimization

A single dosimetric value such as the mean BED is not expected to be predictive of response in tumors that have a nonuniform absorbed dose distribution and, depending on tumor size, a spatially variable radiosensitivity. However, BED remains a reasonable first-order predictor of response for smaller tumors. Moreover, more predictive radiobiologic quantities applicable to larger heterogeneous tumors, such as surviving fraction, EUD, and tumor control probability, are all derived from BED values, typically taken at the voxel level. Thus, any methodology based on BED optimization may easily be extended to

TABLE 1
Radiobiologic Parameters Used

Parameter	NHL	Lungs	Liver	Kidneys
α/β (Gy)	8.6 (*28*)	3.3 (*29*)	2.5 (*30*)	2.6 (*18*)
λ_B (h^{-1})	N/A	0.0106 (*31*)	0.0124 (*31*)	0.0115 (*31*)
λ_Z (h^{-1})	N/A	0.0182 (*32*)	0.00728 (*32*)	0.00957 (*32*)
μ (h^{-1})	1.3 (*33*)	0.46 (*34*)	0.28 (*35*)	0.25 (*18*)

Numbers in parentheses indicate reference from which value was taken.

those other, more comprehensive radiobiologic parameters. As a first-order single-value response or activity escalation criterion, the BED is superior to administrated activity or even absorbed dose.

The expression for the tumor BED is a variation of Equation 6 where the subscript *tum* denotes tumor:

$$BED_{tum} = \left(A_Z d_{Z,tum} + A_B d_{B,tum}\right)\left(1 + G(\infty)_{tum} \times \frac{A_Z d_{Z,tum} + A_B d_{B,tum}}{\alpha_{tum}/\beta_{tum}}\right). \quad \text{Eq. 9}$$

The values of BED_{tum} as a function of A_B are obtained by substituting the expression for A_Z from the organ-appropriate version of Equation 8 into Equation 9 (i.e., in the example illustrated in Fig. 1B, using the liver constraint [Eq. 8] for $A_B < A_{Bint}$ and the lung constraint [Eq. 8] for $A_B \geq A_{Bint}$, we may obtain the dependence of the tumor BED as a function of A_B and thus the optimal value for A_B [and consequently A_Z]). The calculation of $G(\infty)_{tum}$ is no longer trivial, however, because it depends on the sum of the contributions from both the ^{131}I-tositumomab (B) and the ^{90}Y-ibritumomab tiuxetan (Z) whose uptake in tumor are typically best described as a 2-component exponential fit:

$$\dot{D}(t) = \dot{D}_{0,B}(1 - e^{-\kappa_B t})e^{-\lambda_B t} + \dot{D}_{0,Z}(1 - e^{-\kappa_Z t})e^{-\lambda_Z t}, \quad \text{Eq. 10}$$

where the κ parameters are the uptake constants, typically on the order of 24–48 h. Although the biologic uptake and clearance rates may be assumed to be the same, because ^{131}I and ^{90}Y have different physical half-lives, the κ and λ values will be different for each isotope. For purposes of illustration, we will assume a biologic half-life, $T_{\lambda bio}$, of 4 d and a biologic uptake, $T_{\kappa bio}$, of 48 h, values typically seen in clinical dosimetry, and the ^{131}I and ^{90}Y dose rate constants may be calculated using:

$$\left\{\begin{array}{l} \lambda_i = \dfrac{ln2}{T_{\varphi_i}} + \dfrac{ln2}{T_{\lambda bio}} \\ \kappa_i = \dfrac{ln2}{T_{\varphi_i}} + \dfrac{ln2}{T_{\kappa bio}} \end{array}\right\}, \quad \text{Eq. 11}$$

where the index i is valid for both B and Z, and $T_{\phi i}$ is the physical half-life of the isotope (64.0 h for Z [^{90}Y] and 8.02 d for B [^{131}I]). The parameters $\dot{D}_{0,i}$ may be solved for by integrating the 2 terms in Equation 10 separately, giving:

$$\dot{D}_{0,i} = D_i \frac{\lambda_i(\lambda_i + \kappa_i)}{\kappa_i}, \quad \text{Eq. 12}$$

where D_i is the absorbed dose for the isotope i. The values for D_i are taken from the literature (*24,25*) and are listed in Table 2 as d_{tum}, the absorbed dose per unit activity, along with the normal-organ parameters. By substituting Equation 10 into Equation 3, the G-factor may be obtained and then the value calculated numerically (*26*).

The tumor BED as a function of A_B is illustrated in Figure 2 for the same case as shown in Figure 1B (case 1) and using the same normal-organ parameters; further examples are given in the results section in Table 3 and Figure 3 for a range of input values obtained from the same patient datasets whose normal-organ parameters are given in Table 2. The MTBED values are the same as previously given for the lungs and liver; the kidney MTBED is taken to be 28 Gy. The illustrations include A_{Blow} and A_{Bhigh} values, which are the ^{131}I-tositumomab AAs that bracket the range for which the tumor will receive 95% of the maximum BED.

Multiple Tumor Optimization

Because the optimization point depends on tumor kinetics, it is quite possible for a patient with more than one tumor to have different optimal combinations for the different tumors. In these instances, the EUBED (*27*) may be used to optimize the activities relative to multiple tumors. The EUBED is given by:

$$EUBED = -\frac{1}{\alpha} ln\left(\frac{\sum_{i=1}^{N} e^{-\alpha BED_i}}{N}\right), \quad \text{Eq. 13}$$

for N equally contributing components (voxels, for example) of a single tumor. This expression may easily be extended to several tumors:

$$EUBED = -\frac{1}{\alpha} ln\left(\frac{\sum_{i=1}^{N} w_i e^{-\alpha BED_i}}{\sum_{i=1}^{N} w_i}\right), \quad \text{Eq. 14}$$

where the weighting factor, w_i, is proportionate to the preponderance (mass, m) of the tumor, and i now iterates over the number of tumors, N. This approach is illustrated by considering 4 tumors using the case 1 normal-organ kinetics.

The normal-organ parameters are the same for all tumors, because they are from the same patient (Table 2, case 3). The tumor parameters are given in Table 4 and are chosen from within the ranges given in the literature. The masses were arbitrarily attributed for illustrative pur-

TABLE 2
Parameters for Tumor BED-Based Optimization

Parameter (Gy/GBq)	Case 1	Case 2	Case 3	Case 4	Case 5
d_{BLi}	0.97	1.01	0.87	0.87	0.87
d_{ZLi}	6.21	10.46	3.84	3.84	8.81
d_{BLu}	1.20	1.32	0.97	1.32	1.20
d_{ZLu}	2.85	2.44	3.03	3.35	2.70
d_{BKi}	0.72	0.98	0.55	0.55	0.98
d_{ZKi}	2.85	2.73	2.73	2.73	4.05
d_{Btum}	2.50	2.50	2.00	3.0	3.0
d_{Ztum}	10.0	10.0	12.0	10.0	10.0

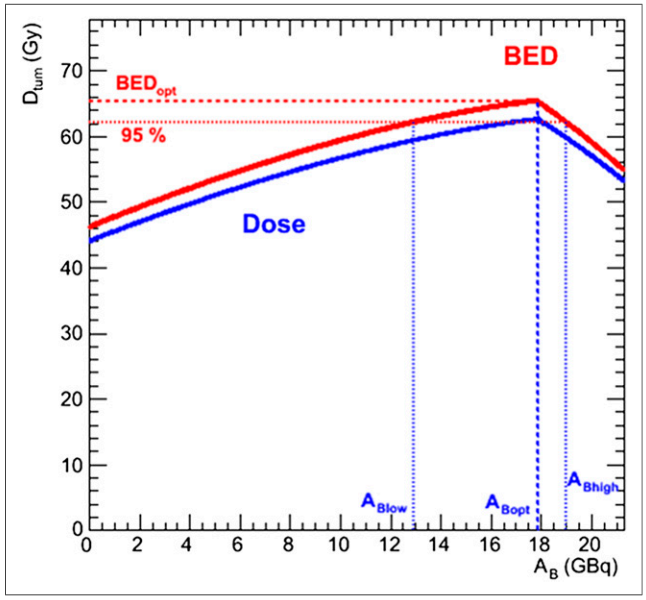

FIGURE 2. Illustration of tumor BED-based optimization (case 1). Tumor dose and BED are plotted as function of A_B. Here, optimal A_B (and A_Z) values (A_{Bopt}, A_{Zopt}) are same as intersection values (A_{Bint}, A_{Zint}).

TABLE 3
Results for Tumor BED-Based Optimization

Quantity	Case 1	Case 2	Case 3	Case 4	Case 5
A_{Bmax} (GBq)	21.3	19.4	26.3	19.4	21.3
A_{Bint} (GBq)	17.9	18.0	11.3	—	17.0, 20.4
A_{Bopt} (GBq)	17.9	17.9	2.40	3.93	17.1
95% range	12.9–19.0	15.8–18.5	0.0–12.1	0.0–12.0	15.7–21.0
A_{Zmax} (GBq)	4.41	2.62	7.14	7.14	3.11
A_{Zint} (GBq)	1.82	0.98	5.15	—	0.50, 1.62
A_{Zopt} (GBq)	1.82	0.98	6.77	5.97	1.64
95% range	1.24–2.71	0.59–1.24	4.90–7.14	3.30–7.14	0.15–1.82
BED_{li} (Gy)	35.0	35.0	35.0	31.9	35.0
BED_{lu} (Gy)	30.0	30.0	27.7	30.0	28.0
BED_{ki} (Gy)	20.9	24.9	24.0	21.8	28.0
AD_{tum} (Gy)	62.7	54.6	86.1	71.5	67.6
BED_{tum} (Gy)	65.4	56.6	93.7	76.4	70.6

poses. The optimization process is essentially the same as for a single tumor: because A_B varies from 0 to A_{Bmax}, the appropriate organ-specific version of Equation 8 for A_Z is substituted into Equation 9 for each tumor. Once the different tumor BEDs are calculated, the disease EUBED is obtained using Equation 14 and the results are plotted, from which the optimal A_{Bopt} (and then A_{Zopt}) value is determined.

RESULTS

MTD Intersection Points and Optimal Activities

By considering sets of data from twelve ^{90}Y-ibritumomab tiuxetan (from myeloablative NHL therapy (*21*)) and five ^{131}I-tositumomab (from nonmyeloablative NHL (*20*)) patients for whom lung and liver kinetics were available, we calculated the intersection points (A_{Bint}, A_{Zint}) for all 60 possible patient data combinations and the optimal tumor BED points (A_{Bopt}, A_{Zopt}) using the average tumor d values reported in the literature (14.9 mGy/MBq for ^{90}Y-ibritumomab tiuxetan and 3 mGy/MBq for ^{131}I-tositumomab) (*24,25*).

The average A_{Bint} value was 19.0 ± 8.2 GBq (range, 3.9–36.9 GBq), and the average tumor dose contribution from ^{131}I-tositumomab was 57.0 ± 24.4 Gy; the average A_{Zint} value was 2.77 ± 1.64 GBq (range, 0.42–7.54 GBq), and the average tumor dose contribution from ^{90}Y-ibritumomab tiuxetan was 41.3 ± 24.5 Gy for MTBEDs of 30 and 35 Gy for the lung and liver, respectively. Eleven of the 60 scenarios showed a ^{90}Y contribution of less than the maximum-allowed nonmyeloablative activity of 1.18 GBq using the MTBED constraints alone. When tumor BED optimization was obtained, the average A_{Bopt} value was 18.0 ± 9.2 GBq (range, 0.1–36.8 GBq) and the average A_{Zopt} value was 2.75 ± 1.63 GBq (range, 0.43–10.2 GBq), and 10 of the 60 scenarios required the administration of less than maximum-allowed nonmyeloablative ^{90}Y-ibritumomab tiuxetan activity. However, the point of such a methodology is not to obtain average values but to personalize the therapy to the individual patient. Thus, it is important to notice that although, on average, the contribution from ^{131}I-tositimomab may have been higher, the amount of optimal activity of ^{90}Y-ibritumomab tiuxetan was greater than the maximum-allowed activity for nonmyeloablative single therapeutic therapy in 50 of 60 cases, with a maximum nearly 12 times that of the standard activity, and in 24 cases the ^{90}Y contributed more AD (and BED) to the tumor than the ^{131}I.

Tumor BED Optimization

Several different scenarios have been chosen to illustrate the different possible cases that may arise and to show the greater detail available through this methodology, which may inform a clinical decision regarding the quantities of activity to administer beyond the simple calculation of a single (A_{Bopt}, A_{Zopt}) optimization point. The results are shown in Table 3 and are graphed in Figure 3, in addition to those already shown in Figures 1 and 2. Case 1 represents the average values from the patient data and is the methodologic example illustrated in Figures 1 and 2. Case 2 is a typical example, with results similar to the mean values (case 1) but using data from individual ^{131}I-tositumomab and ^{90}Y-ibritumomab tiuxetan data. Case 3, illustrated in Figures 3C and 3D, shows a case in which the tumor BED optimization point differs from the MTBED intersection point. Case 4 shows an example of no intersection point: here the lungs are the constraining organ for all activity combinations (Figs. 3E and 3F). Case 5 shows an example of 3 organs constraining the activity—the lungs, liver, and kidneys; there are 2 intersection points, 1 of which is also the optimization point. The last 2 cases are somewhat contrived and did not occur naturally using the patient dataset at the MTBED values (30 Gy for lungs, 35 Gy for liver, 28 Gy for kidneys); the kinetics values used for the normal organs have been taken from different patients to create the desired scenarios. However, given a sufficiently large number of patients, it is indeed possible that these scenarios would occur, thus their inclusion.

Multiple Tumor Optimization

The tumor dose per AA for the different tumors was judiciously chosen to illustrate a case where no 2 tumors individually had the same optimization point. The optimization was implemented for each tumor separately (Table 5), and at each (A_B, A_Z) point the EUBED was calculated. The results are also graphed in Figure 4. Figure 4B is an enlargement of the EUBED results and shows the range using the 95% of maximum EUBED threshold.

DISCUSSION

The significance of the proposed methodology is 3-fold: the inclusion of radiobiologic quantities for normal-organ constraints (BED) and the tumor target (EUBED), widely regarded as more relevant to biologic endpoints; the graphical representation of the results, which allows for easy understanding of quantitative effects of deviations from the optimal solutions (i.e., the knowledge of how much tumor BED is lost by choosing different AAs is available); and the development of the model within the context

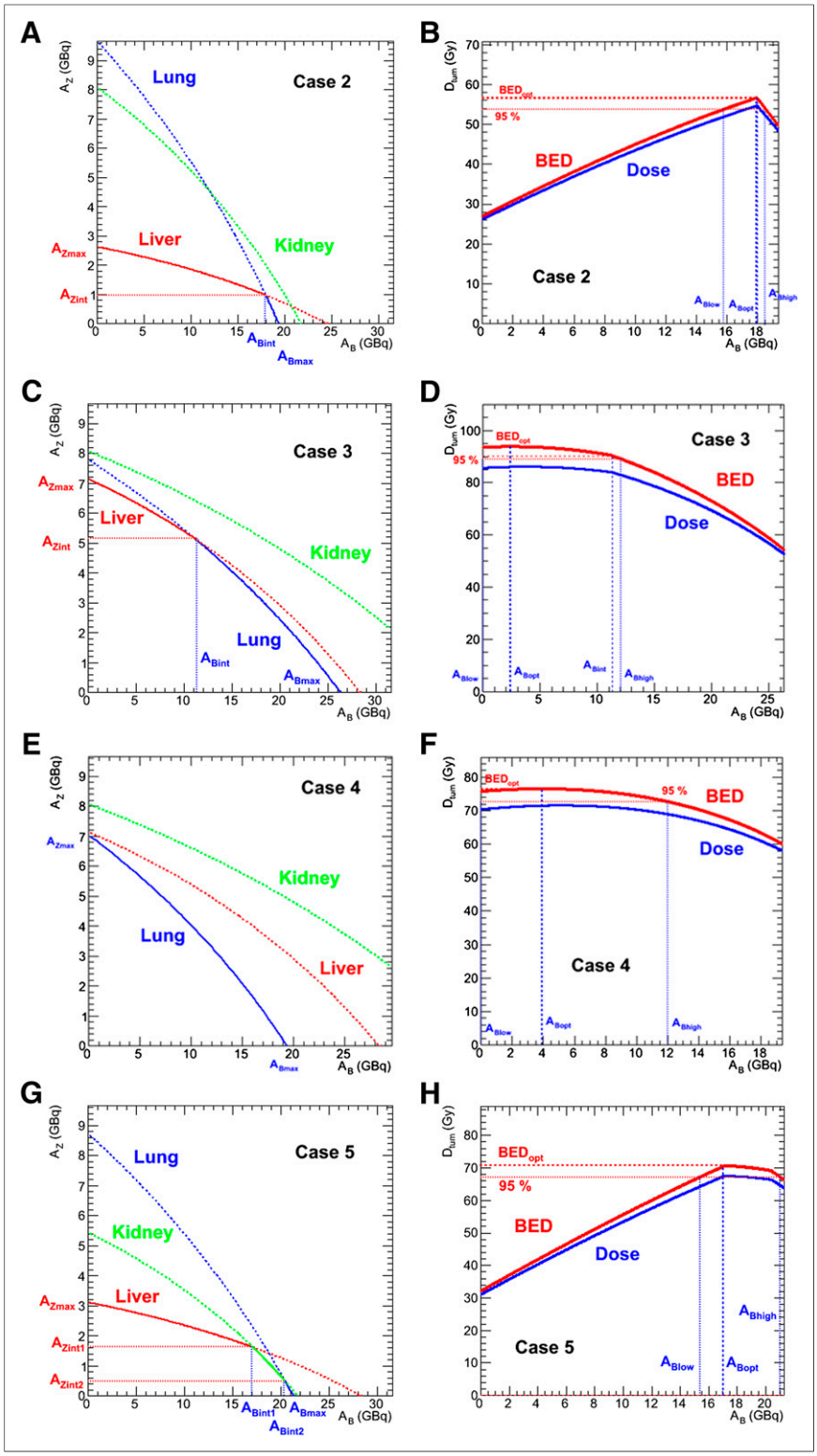

FIGURE 3. Illustration of different cases. Case 3 (C and D) shows constraints and tumor BED for example where optimal dosing is not equal to intersection of MTD constraints. Case 4 (E and F) shows case for single limiting organ. Case 5 (G and H) illustrates case where all 3 organ constraints must be considered.

of a functional 3D dosimetry software package, 3D-RD, with the ability to implement sophisticated methodologies within clinical time frames (*19*). Concerning the graphical representation, we have chosen to show the administrative activity limits, A_{Blow} and A_{Bhigh}, which correspond to a threshold where the tumor BED (or the EUBED) is at 95% of the maximum. Clearly, this is an arbitrary threshold that can be varied; however, it serves to illustrate the point that a graphical representation allows for a better understanding of the effect of varying the ratio of A_B to A_Z. To accomplish the objective of clinical implementation, several other technical difficulties must be overcome, some of which are discussed.

A clinical consideration for this dual-isotope myeloablative methodology is the choice of procedure for the myeloablation. Cyclophosphamide combined with 300 cGy total-body irradiation is a widely used myeloablative conditioning regimen for autologous and allogeneic stem cell transplant. However, for this particular combination, cold antibody tositumomab in conjunction with the cyclophosphamide would be preferable to total-body irradiation. The cold antibody would be given before cyclophosphamide to minimize the window between administration of radioactive drugs and infusion of the autograft (the timing of which is based on the estimated radiation dose rate in the blood and bone marrow (*21*)).

The accurate calculation of the dosimetric quantities needed for the model depends critically on the ability to measure the quantities of the pretherapeutic activities (^{111}In-ibritumomab tiuxetan, used as a surrogate for ^{90}Y-ibritumomab tiuxetan, and ^{131}I-tositumomab) present simultaneously in the patient through quantitative (SPECT) imaging. This dual-isotope imaging requires using multiple-energy-window imaging with correction for cross-talk from the higher-energy ^{131}I γ-rays into the mid-energy ^{111}In energy range. Simulation and phantom studies are currently under way to optimize the reconstruction method and determine the optimal timing and activity ratios of the ^{111}In and ^{131}I agent planning injections to achieve accurate organ dose estimates. From these studies, the requisite sequence of delivery of ^{131}I and ^{111}In radioantibodies will be determined.

This method is designed to serve as a guide to AAs of the agents; during implementation it is clear that clinical or practical considerations may override the suggested AAs. Such considerations may include availability of large amounts of one of the radiopharmaceuticals, concerns over radiation safety issues from large quantities of ^{131}I, and the desire for a minimum AA for one or both radiopharmaceuticals. An advantage of this method is the ability to visually quan-

TABLE 4
Parameters for Disease EUBED-Based Optimization

Parameter	Tumor 1	Tumor 2	Tumor 3	Tumor 4
d_{Btum} (Gy/GBq)	2.5	2.0	3.0	1.6
d_{Ztum} (Gy/GBq)	10.0	12.0	14.0	10.0
m_{tum} (g)	10	12	5	25

tify how such clinical or practical considerations might affect the dosimetric endpoint and better enable the treating physician to balance the different considerations when choosing the therapeutic AAs. A further caveat is that although the optimization is radiobiologically driven and personalized, many clinical personal factors are not taken into consideration and the clinical outcomes may be different.

One of the motivations for combining these 2 radiopharmaceuticals is the different average range of the emitted ionizing radiation (~1 mm with ^{131}I, ~3–5 mm with ^{90}Y), indicating that the 2 isotopes are optimally suited for treating different tumor sizes (2.6–5.0 mm for ^{131}I and 2.8–4.2 cm for ^{90}Y) (*2*). This facet has not been explicitly factored into the current method, because the relative advantages of the 2 isotopes for tumors are limited to direct dosimetric measurements of whole tumors from the patient images. However, this method considers only visible tumor sites, whereas in lymphoma one may expect a distribution of tumor sizes, spanning from clinically observable lesions that are more than 2 cm in diameter to occult disease that is below the resolution of current imaging modalities. Although the optimal tumor size distribution for ^{90}Y is at the limit of detectability and may or may not appear in SPECT/CT images, it is clear that the optimal tumor size distribution for ^{131}I is well below the conventional imaging threshold of detectability. In addition, the ^{131}I provides a nonnegligible dose to the whole body, including all tumors, from the photon emissions. For these reasons, it may indeed be preferable to include a minimum ^{131}I-tositumomab constraint in the optimization. A possible extension of the model would include quantification of the number and size distribution of invisible disease and the use of Monte Carlo to integrate the treatment optimization of the microscopic tumor distribution with the macroscopic measurable tumors.

TABLE 5
Results for Tumor BED-Based Optimization

Quantity	Tumor 1	Tumor 2	Tumor 3	Tumor 4	Combined
A_{Bopt} (GBq)	17.9	12.2	17.9	11.3	15.3
A_{Zopt} (GBq)	1.81	2.84	1.81	2.99	2.30
BED_{tum1} (Gy)	54.6*	49.3	54.6*	48.3	52.4
BED_{tum2} (Gy)	59.8	61.2*	59.8	61.1	60.8
BED_{tum3} (Gy)	83.3*	80.9	83.3*	80.2	82.6
BED_{tum4} (Gy)	48.2	49.7	48.2	49.8*	49.2
EUBED (Gy)	54.7	54.6	54.7	54.3	55.0*

*Maximum BED values obtained for optimization of respective tumor (e.g., maximum BED for tumor 1 is obtained when optimization is run for tumor 1 itself).

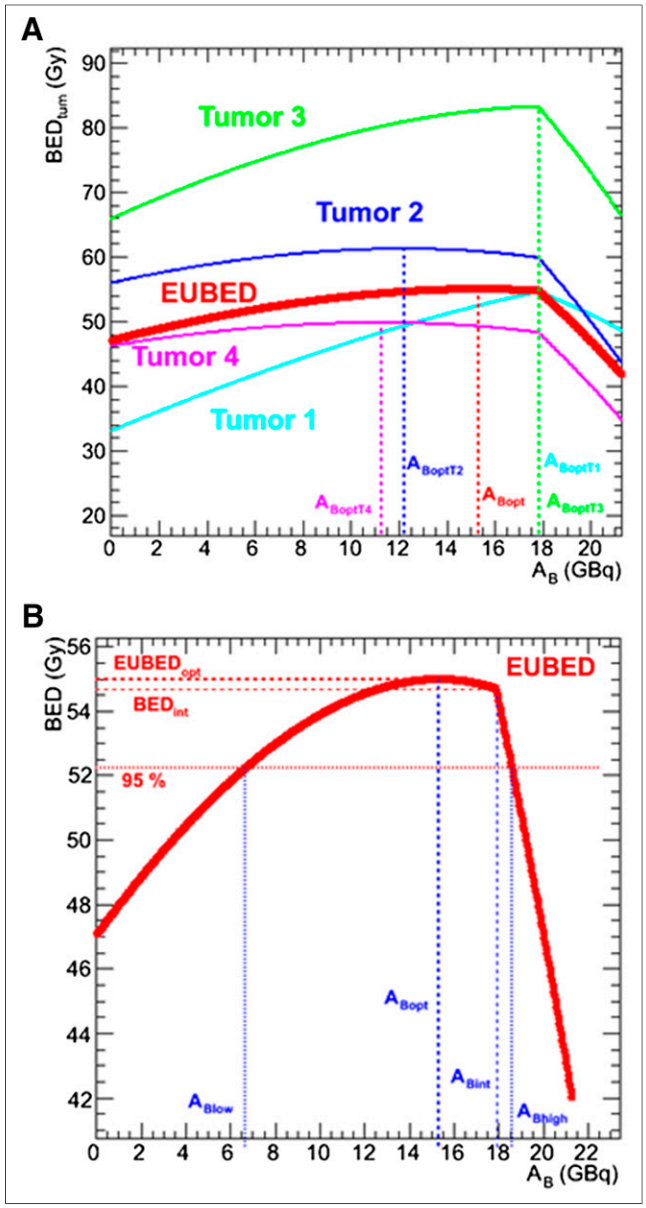

FIGURE 4. Multiple tumor optimization. (A) Optimization for tumors separately in different colors and for EUBED (in red). (B) Enlargement of EUBED curve.

CONCLUSION

A rational approach for combination radiopharmaceutical treatment has been developed and applied to the myeloablative treatment of NHL. The methodology outlined provides a rigorous, dosimetry-driven and radiobiologically based path toward combination radiopharmaceutical therapy.

DISCLOSURE

The costs of publication of this article were defrayed in part by the payment of page charges. Therefore, and solely to indicate this fact, this article is hereby marked "advertisement" in accordance with 18 USC section 1734. Dr. Richard Wahl holds patents on both ^{131}I-tositumomab and ^{90}Y-ibritumomab tiuxetan and receives royalties via a licensing agreement when ^{131}I-tositumomab and ^{90}Y-

ibritumomab tiuxetan are used clinically in the United States. He also has received speaker fees from GlaxoSmithKline. No other potential conflict of interest relevant to this article was reported.

REFERENCES

1. Kotzerke J, Bunjes D, Scheinberg DA. Radioimmunoconjugates in acute leukemia treatment: the future is radiant. *Bone Marrow Transplant.* 2005;36:1021–1026.
2. O'Donoghue JA, Bardies M, Wheldon TE. Relationships between tumor size and curability for uniformly targeted therapy with beta-emitting radionuclides. *J Nucl Med.* 1995;36:1902–1909.
3. Walrand S, Hanin FX, Pauwels S, Jamar F. Tumour control probability derived from dose distribution in homogeneous and heterogeneous models: assuming similar pharmacokinetics, ^{125}Sn-^{177}Lu is superior to ^{90}Y-^{177}Lu in peptide receptor radiotherapy. *Phys Med Biol.* 2012;57:4263–4275.
4. Villard L, Romer A, Marincek N, et al. Cohort study of somatostatin-based radiopeptide therapy with [^{90}Y-DOTA]-TOC versus [^{90}Y-DOTA]-TOC plus [^{177}Lu-DOTA]-TOC in neuroendocrine cancers. *J Clin Oncol.* 2012;30:1100–1106.
5. Kunikowska J, Krolicki L, Hubalewska-Dydejczyk A, Mikolajczak R, Sowa-Staszczak A, Pawlak D. Clinical results of radionuclide therapy of neuroendocrine tumours with ^{90}Y-DOTATATE and tandem ^{90}Y/^{177}Lu-DOTATATE: which is a better therapy option? *Eur J Nucl Med Mol Imaging.* 2011;38:1788–1797.
6. de Jong M, Breeman WA, Valkema R, Bernard BF, Krenning EP. Combination radionuclide therapy using ^{177}Lu- and ^{90}Y-labeled somatostatin analogs. *J Nucl Med.* 2005;46(suppl 1):13S–17S.
7. Frilling A, Weber F, Saner F, et al. Treatment with ^{90}Y- and ^{177}Lu-DOTATOC in patients with metastatic neuroendocrine tumors. *Surgery.* 2006;140:968–976.
8. Seregni E, Maccauro M, Coliva A, et al. Treatment with tandem [^{90}Y]DOTA-TATE and [^{177}Lu]DOTA-TATE of neuroendocrine tumors refractory to conventional therapy: preliminary results. *Q J Nucl Med Mol Imaging.* 2010;54:84–91.
9. Madsen MT, Bushnell DL, Juweid ME, et al. Potential increased tumor-dose delivery with combined ^{131}I-MIBG and ^{90}Y-DOTATOC treatment in neuroendocrine tumors: a theoretic model. *J Nucl Med.* 2006;47:660–667.
10. Witzig TE, Fishkin P, Gordon LI, et al. Treatment recommendations for radioimmunotherapy in follicular lymphoma: a consensus conference report. *Leuk Lymphoma.* 2011;52:1188–1199.
11. Johnson P, Glennie M. The mechanisms of action of rituximab in the elimination of tumor cells. *Semin Oncol.* 2003;30(1, suppl 2):3–8.
12. Witzig TE, Gordon LI, Cabanillas F, et al. Randomized controlled trial of yttrium-90-labeled ibritumomab tiuxetan radioimmunotherapy versus rituximab immunotherapy for patients with relapsed or refractory low-grade, follicular, or transformed B-cell non-Hodgkin's lymphoma. *J Clin Oncol.* 2002;20:2453–2463.
13. Press OW, Eary JF, Badger CC, et al. Treatment of refractory non-Hodgkin's lymphoma with radiolabeled MB-1 (anti-CD37) antibody. *J Clin Oncol.* 1989;7:1027–1038.
14. Krishnan A, Nademanee A, Fung HC, et al. Phase II trial of a transplantation regimen of yttrium-90 ibritumomab tiuxetan and high-dose chemotherapy in patients with non-Hodgkin's lymphoma. *J Clin Oncol.* 2008;26:90–95.
15. Winter JN, Inwards DJ, Spies S, et al. Yttrium-90 ibritumomab tiuxetan doses calculated to deliver up to 15 Gy to critical organs may be safely combined with high-dose BEAM and autologous transplantation in relapsed or refractory B-cell non-Hodgkin's lymphoma. *J Clin Oncol.* 2009;27:1653–1659.
16. Song H, Du Y, Sgouros G, Prideaux A, Frey E, Wahl RL. Therapeutic potential of ^{90}Y- and ^{131}I-labeled anti-CD20 monoclonal antibody in treating non-Hodgkin's lymphoma with pulmonary involvement: a Monte Carlo-based dosimetric analysis. *J Nucl Med.* 2007;48:150–157.
17. Wiseman GA, White CA, Stabin M, et al. Phase I/II ^{90}Y-Zevalin (yttrium-90 ibritumomab tiuxetan, IDEC-Y2B8) radioimmunotherapy dosimetry results in relapsed or refractory non-Hodgkin's lymphoma. *Eur J Nucl Med.* 2000;27:766–777.
18. Barone R, Borson-Chazot F, Valkema R, et al. Patient-specific dosimetry in predicting renal toxicity with ^{90}Y-DOTATOC: relevance of kidney volume and dose rate in finding a dose-effect relationship. *J Nucl Med.* 2005;46(suppl 1):99S–106S.
19. Hobbs RF, Wahl RL, Lodge MA, et al. ^{124}I PET-based 3D-RD dosimetry for a pediatric thyroid cancer patient: real-time treatment planning and methodologic comparison. *J Nucl Med.* 2009;50:1844–1847.
20. Jacene HA, Filice R, Kasecamp W, Wahl RL. Comparison of ^{90}Y-ibritumomab tiuxetan and ^{131}I-tositumomab in clinical practice. *J Nucl Med.* 2007;48:1767–1776.
21. Frey E, He B, Sgouros G, Flinn I, Wahl R. Estimation of post-therapy marrow dose rate in myeloablative Y-90 ibritumomab tiuxetan therapy [abstract]. *J Nucl Med.* 2006;47(suppl 1):156P.
22. Dale RG. The application of the linear-quadratic dose-effect equation to fractionated and protracted radiotherapy. *Br J Radiol.* 1985;58:515–528.
23. Fowler JF. The linear-quadratic formula and progress in fractionated radiotherapy. *Br J Radiol.* 1989;62:679–694.
24. Rizvi SN, Visser OJ, Vosjan MJ, et al. Biodistribution, radiation dosimetry and scouting of ^{90}Y-ibritumomab tiuxetan therapy in patients with relapsed B-cell non-Hodgkin's lymphoma using ^{89}Zr-ibritumomab tiuxetan and PET. *Eur J Nucl Med Mol Imaging.* 2012;39:512–520.
25. Sgouros G, Squeri S, Ballangrud AM, et al. Patient-specific, 3-dimensional dosimetry in non-Hodgkin's lymphoma patients treated with ^{131}I-anti-B1 antibody: assessment of tumor dose-response. *J Nucl Med.* 2003;44:260–268.
26. Hobbs RF, Sgouros G. Calculation of the biological effective dose (BED) for piece-wise defined dose-rate fits. *Med Phys.* 2009;36:904–907.
27. O'Donoghue JA. Implications of nonuniform tumor doses for radioimmunotherapy. *J Nucl Med.* 1999;40:1337–1341.
28. Aref A, Mohammad R, Yudelev M, et al. Radiobiological characterization of two human chemotherapy-resistant intermediate grade non-Hodgkin's lymphoma cell lines. *Radiat Oncol Investig.* 1999;7:158–162.
29. Van Dyk J, Mah K, Keane TJ. Radiation-induced lung damage: dose-time-fractionation considerations. *Radiother Oncol.* 1989;14:55–69.
30. Cremonesi M, Ferrari M, Bartolomei M, et al. Radioembolisation with ^{90}Y-microspheres: dosimetric and radiobiological investigation for multi-cycle treatment. *Eur J Nucl Med Mol Imaging.* 2008;35:2088–2096.
31. Hobbs RF, Baechler S, Wahl RL, et al. Arterial wall dosimetry for non-Hodgkin lymphoma patients treated with radioimmunotherapy. *J Nucl Med.* 2010;51:368–375.
32. He B, Wahl RL, Sgouros G, et al. Comparison of organ residence time estimation methods for radioimmunotherapy dosimetry and treatment planning–patient studies. *Med Phys.* 2009;36:1595–1601.
33. Bodey RK, Flux GD, Evans PM. Combining dosimetry for targeted radionuclide and external beam therapies using the biologically effective dose. *Cancer Biother Radiopharm.* 2003;18:89–97.
34. Brenner DJ, Hall EJ. Conditions for the equivalence of continuous to pulsed low dose rate brachytherapy. *Int J Radiat Oncol Biol Phys.* 1991;20:181–190.
35. Krishnan S, Lin EH, Gunn GB, et al. Conformal radiotherapy of the dominant liver metastasis: a viable strategy for treatment of unresectable chemotherapy refractory colorectal cancer liver metastases. *Am J Clin Oncol.* 2006;29:562–567.